Production of Polystyrene Particles via Aerosolization

SOMCHINTANA NORASETTHEKUL,[1] AHMED M. GADALLA,[1,*] and HARRY J. PLOEHN[2,†]

[1]Department of Chemical Engineering, Texas A&M University, College Station, Texas 77843-3122, and
[2]Department of Chemical Engineering, University of South Carolina, Swearingen Engineering Center, Columbia, South Carolina 29208

SYNOPSIS

Aerosolization of polystyrene solutions followed by drying in a tubular furnace produced submicron-sized polystyrene particles. Characterization using x-ray diffraction, scanning electron microscopy (SEM), and infrared spectroscopy (FT-IR) revealed that the particles were amorphous, spherical, and free of residual solvent. The average particle size and size distribution varied with furnace temperature, the initial polystyrene solution concentration, and solvent type. The particles' BET-based specific surface area depended upon these parameters as well as the carrier gas flow rate. Analysis of the competing rates of convection, solvent evaporation, droplet collisions, and polymer diffusion help to rationalize the results. The dependence of the solvent evaporation rate on temperature controls the particle diameter, but droplet coalescence cannot be ignored. Long residence times and high furnace temperatures softened the particles; after filtration, polymer diffusion between solid particles produced visual evidence of partial coalescence. © 1995 John Wiley & Sons, Inc.

INTRODUCTION

Aerosolization, the dispersion of colloidal solid particles or liquid droplets in a gas, provides an efficient means of producing powders with controlled characteristics and excellent purity. Ideal powders for ceramic applications have spherical morphologies, high homogeneity and purity, and fine grain size with narrow size distributions.[1-5] The same features are useful in applications involving polymer particles. Unlike precipitation of solid particles from liquid solutions, aerosolization can confine multiple solutes within small droplets that can be rapidly dried, minimizing chemical segregation. This feature may give aerosolization an advantage in the production of polymer blends or other polymer–solute mixtures. For this reason, we have explored aerosolization as a means of producing polymer particles with controlled characteristics.

Aerosols can be produced either by evaporation–condensation or atomization. In evaporation–condensation, condensation of a solute nucleates particles from the vapor phase. The product particles have a relatively narrow size distribution, but the process may allow chemical segregation and is certainly not feasible for direct production of particles composed of polymers or other nonvolatile materials. Atomization produces aerosols by physical dispersion of liquid into droplets. Of the many types of atomizers,[6,7] most produce droplets, and ultimately solid particles, with broad size distributions.

Atomization can produce polymer particles by two distinct routes. Monomer can first be atomized to produce droplets, followed by polymerization via a vapor phase initiator.[8-10] This method offers the possibility of producing polymer particles from monomers that cannot be polymerized by other methods. Each monomer droplet acts as a separate reactor that facilitates heat transfer with the gas phase. Spherical particles of poly(*p-tert* butylstyrene)[8], polystyrene,[9] and polyurea[10] have been produced in this way, often with narrow size distributions. However, polydisperse or irregular particles sometimes resulted from incomplete reaction of the monomers.

Alternately, polymer solution can first be atomized, followed by solvent evaporation (i.e., spray drying). Bhanti et al.[11] generated radioactively

* Deceased.
† To whom correspondence should be addressed.

Journal of Applied Polymer Science, Vol. 58, 2101–2110 (1995)
 CCC 0021-8995/95/112101-10

tagged aerosol droplets by atomizing solutions of polystyrene and ^{51}Cr in xylene using a nebulizer, followed by solvent evaporation in air. The spherical, polydisperse particles were subsequently separated into nearly monodisperse size groups using an aerosol centrifuge. Mathiowitz et al.[12] used spray drying to produce bioerodible polyanhydride particles for drug delivery applications. The product particles had irregular shapes and were more amorphous than the original polymers, presumably because rapid drying left little time for polymer molecules to assume crystalline order.

Chiang and Prud'homme[13] produced monodisperse polystyrene particles by means of forced capillary jet breakup with flow disturbances driven by a piezo-electric crystal. Some of the particles had dimpled morphologies: diffusion-limited transport of the solvent from the particle interior led to the formation of a hard outer shell that collapsed with further solvent evaporation. Higher drying temperatures or use of plasticizing cosolvents produced smoother particles. Drying at a temperature below polystyrene's glass transition temperature (105°C) prevented particle aggregation to form doublets, but plasticizing cosolvents increased the number of doublets.

We are not aware of any careful studies of polymer solution spray drying that relate the average particle diameter and its distribution to process conditions. To improve our understanding of this relationship, we have studied the production of polystyrene particles by spray drying. We varied the concentration of the initial PS solution, the furnace temperature, the carrier gas flow rate, and solvent composition to characterize their influence upon particle morphology, average diameter, diameter distribution, purity, pore volume, surface area, and crystallinity.

EXPERIMENTAL

Materials

We used commercial grade polystyrene (PS) (Aldrich) with two different average molecular weights (280,000 and 45,000 g/mol) to prepare solutions in benzene, toluene, a mixture containing benzene plus 10% v/v methanol, and a mixture of benzene plus 25% v/v isopropanol (all solvents from Baker Analyzed). Nitrogen gas (Bob Smith Co.) was used as received.

Particle Synthesis

Our synthesis of PS particles employed the bench scale apparatus shown in Figure 1. A six-jet atomizer (Thermal Systems Model 9306) was used to atomize the PS solutions. The flow of compressed nitrogen gas (20 psig for all experiments) through a 0.38 mm orifice created a pressure drop that drew the PS solution up into the atomizer. The nitrogen flow entrained the solution to create an aerosol with a distribution of drop sizes. The atomizer jet then impinged upon a spherical impactor; large drops collided with the impactor and returned to the reservoir, but small drops passed out of the atomizer. Additional nitrogen gas was admitted at the atomizer exit and carried the droplets into the tube furnace. The use of nitrogen avoided oxidation and decreased the possibility of combustion.

A 32.5 cm long, 3 cm diameter Vycor glass tube with a 90° elbow carried the aerosol from the atomizer to the tubular furnace. The tubular furnace consisted of a 3 cm diameter, 91 cm long Vycor glass tube encased in two semicircular electric heating units (61 cm in length) operable up to 1500 K. A temperature controller (Omega Model 4001-KC) maintained the temperature of the furnace in conjunction with a K-type thermocouple placed at the midlength of the glass tube on the exterior surface. Other portions of the vents, tube, and filter holder were wrapped with electrical heating tape to prevent condensation of solvent inside the apparatus. The thermocouple reading was calibrated to estimate the

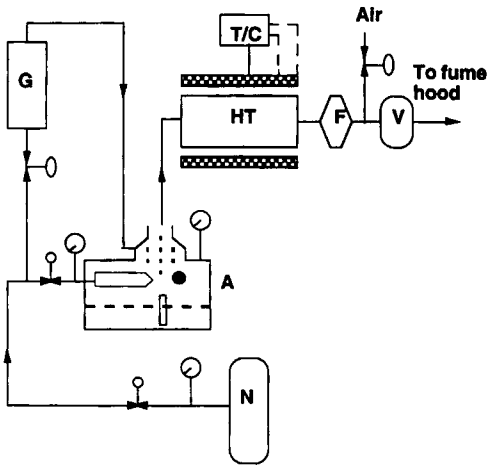

Figure 1 Schematic diagram of the aerosolization apparatus, including atomizer and tube furnace. Components are labelled as follows: N, nitrogen cylinder; A, atomizer; G, gas flow meter; HT, heating unit and tubular furnace; T/C, temperature controller; F, filter; and V, vacuum pump.

axial temperature profile along the centerline of the furnace.

A filter system at the end of the tubular furnace collected the product particles. We mounted a Nucleopore polycarbonate filter membrane with 0.2 μm pore size (Costar) in a filter holder connected to a vacuum pump. To prevent pressurization of the tubular furnace as particles accumulated on the filter, we used a vacuum pump to maintain a constant flow rate of carrier gas. The solvent-laden carrier gas was vented to a fume hood. The process was stopped every 30 min in order to collect particles from the filter membrane.

Characterization

Particle Size, Size Distribution, and Internal Morphology

We used scanning electron microscopy (JEOL JSM-6400) to visualize the product particles. Ultrasonic agitation dispersed the particles in ethanol followed by vacuum drying. After mounting on aluminum stubs and gold coating, the samples were imaged and photographed. We constructed particle size distributions by measuring and tabulating individual particle sizes; in all but two cases, we sized more than 500 particles per sample.

To investigate the internal morphology of product particles, we used a special specimen preparation procedure. Mixing particles with an epoxy resin, followed by curing, firmly embedded the particles in a solid matrix. The specimens were cut by microtome to expose particle interiors. The microtomed surfaces were imaged by SEM and photographed.

BET Nitrogen Adsorption

Adsorption of nitrogen and BET analysis provided specific surface areas and pore volumes of the product PS particles. Degassing at low pressure removed any initial adsorbate from the samples. An automated instrument, the Digisorb 2600 (Micrometrics), measured the amount of gas adsorbed as a function of pressure. This data was interpreted according the BET equation[14] to calculate the specific surface area.

Other Chemical and Physical Characterization

To identify the presence of residual solvents in the particles, we used Fourier Transform Infrared Spectroscopy (FT-IR; IBM Instruments FT-IR/Series 32). Samples were mixed with KBr, ground, pelletized, and mounted in the spectrometer. We characterized the degree of crystallinity using x-ray diffraction (Scintag Model DMS 2000) using a copper target with a nickel filter.

The viscosities of solvents and solutions were measured using a thermostatted Ostwald capillary viscometer (Sargent) calibrated with water at 25°C. We used a Du Nouy ring tensiometer (Fisher Model 20) to determine the surface tensions of solvents and polymer solutions. A calibrated liquid pycnometer (Fisher) quantified the density of mixed solvents and the product PS particles.

RESULTS

Particle Morphology

SEM images of epoxy-embedded, microtomed PS particles (Fig. 2, 280,000 g/mol PS; Fig. 3, 45,000 g/mol PS) shows that the particles were solid and apparently homogeneous. The similarity of the measured particle density (between 0.96 and 1.11 g/cm^3) to the usual density of bulk PS (1.04–1.07 g/cm^3) and the low measured pore volume (about 1% of the total particle volume by BET) suggests that the particles had no significant pores.

X-Ray diffraction patterns indicated an amorphous arrangement of the PS molecules in the particles. Considering the rapidity of the drying process (usually much less than 30 s) and the observation that bulk PS is usually amorphous, this result was expected.

We also gathered infrared spectra of the starting dry PS, pure benzene, PS containing small amounts

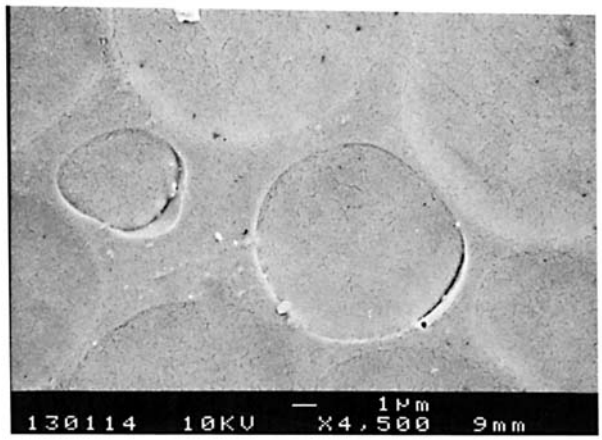

Figure 2 SEM image of microtomed PS particles produced from 0.01 g/cm^3 solution of PS in benzene (T = 114°C, Q = 57 cm^3/s, 280,000 g/mol of average molecular weight, and 4,500× magnification).

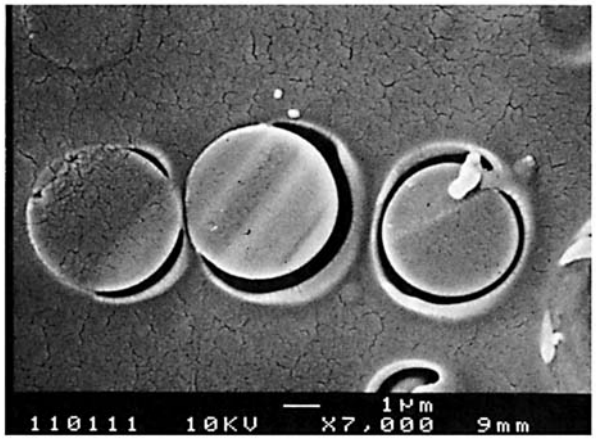

Figure 3 SEM image of microtomed PS particles produced from 0.01 g/cm^3 solution of PS in benzene (T = 114°C, Q = 57 cm^3/s, 45,000 g/mol of average molecular weight, and 7,000× magnification).

of added benzene, and aerosol-derived PS particles. Comparison of these spectra demonstrated that the product PS particles contained no detectable residual benzene.

Particle Diameter and Specific Surface Area

Table I shows the effects of varying furnace temperature (T) and PS concentration in the starting solution ([PS]) on the characteristics of aerosol-derived PS particles. The number-average and area-average particle diameters (D_N and D_A) represent averages over N individual particles. The specific surface area S_{SEM} was calculated from D_A via

$$S_{SEM} = \frac{6}{\rho_{PS} D_A} \quad (1)$$

In Table I, S_{BET} denotes the specific surface area estimated from N_2 adsorption and BET analysis.

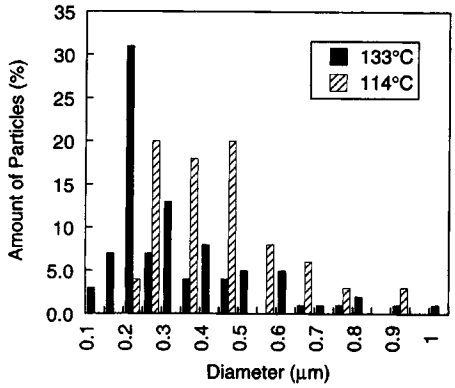

Figure 4 Particle size distributions of PS particles produced from 0.02 g/cm^3 solution of 280,000 g/mol PS in benzene (Q = 124 cm^3/s). Open and filled bars are for T = 114 and 133°C, respectively.

The polydispersity of the particles produced large standard deviations of the diameters and S_{SEM}. Typical particle diameter histograms (Fig. 4) are clearly not normal distributions. Despite the large standard deviations and nonnormal distributions, the large numbers of particles in each histogram maximize the statistical significance of our comparisons. Unless otherwise noted, all comparisons are statistically significant at a 95% or greater level of confidence.

Several effects led to broad particle size distributions (Fig. 4). First, the six-jet atomizer produced a polydisperse distribution of droplets. Second, the droplets collided and coalesced to an unknown extent before the solvent evaporated. Third, polymer diffusion between particles on the filter membrane caused partial particle coalescence.

Effect of Furnace Temperature

Holding [PS] constant, both the number- and area-average diameters of the particles decreased with increasing T (Table I). For [PS] = 0.02 g/cm^3, D_N

Table I Effect of Furnace Temperature and PS Concentration on Particle Characteristics[a]

T (°C)	[PS] (g/cm^3)	N	D_N (μm)	D_A (μm)	S_{SEM} (cm^2/g)/10^4	S_{BET} (cm^2/g)/10^4	$\frac{S_{SEM}}{S_{BET}}$
114	0.01	294	0.49 ± 0.47	0.68 ± 0.50	8.40 ± 6.18	5.30 ± 0.03	1.59
114	0.02	548	0.66 ± 0.70	0.96 ± 0.76	5.95 ± 4.71	4.44 ± 0.02	1.34
114	0.025	798	0.72 ± 0.57	1.06 ± 0.65	5.39 ± 3.31	4.16 ± 0.05	1.30
133	0.02	594	0.41 ± 0.41	0.58 ± 0.45	9.85 ± 7.64	4.08 ± 0.08	2.41
133	0.025	1050	0.45 ± 0.41	0.61 ± 0.44	9.37 ± 6.76	3.12 ± 0.13	3.00
133	0.03	1256	0.54 ± 0.52	0.75 ± 0.57	7.62 ± 5.79	2.16 ± 0.02	3.53

[a] All produced using 124 cm^3/s carrier gas flow rate.

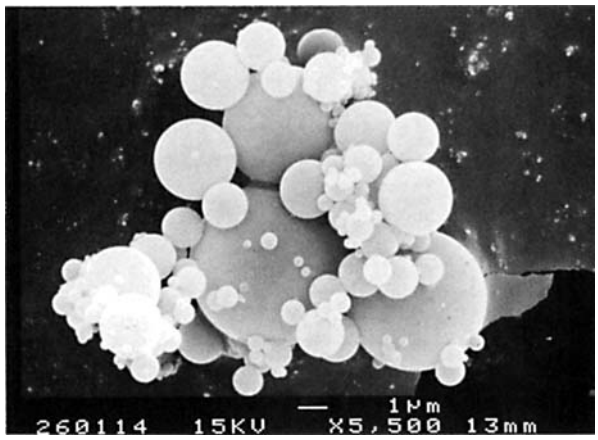

Figure 5 SEM image of PS particles produced from a solution of 280,000 g/mol PS in benzene ([PS] = 0.02 g/cm^3, Q = 124 cm^3/s, T = 114°C,and 5,500× magnification).

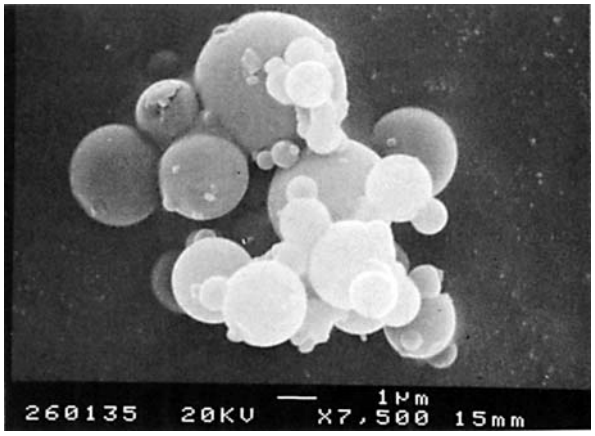

Figure 6 SEM image of PS particles produced from a solution of 280,000 g/mol PS in benzene ([PS] = 0.02 g/cm^3, Q = 124 cm^3/s, T = 133°C, and 7,500× magnification).

decreased from 0.66 μm to 0.41 μm for an increase in T from 114 to 133°C; for [PS] = 0.025 g/cm^3 and the same temperatures, D_N decreased by the same percentage.

The furnace temperature also affected particle morphologies. At T = 114°C, the particles were spherical and unagglomerated (Fig. 5). At higher temperatures (133°C, Fig. 6; 147°C, Fig. 7), the particles agglomerated and started to lose their spherical shape. Partial interparticle coalescence, or sintering, can be seen in the formation of necks between particles.

The specific surface areas calculated from the area-average particle diameter (S_{SEM}, Table I) increased with T; the corresponding decrease in D_A accounts for this trend. However, the specific surface area obtained from nitrogen adsorption with BET analysis (S_{BET}, Table I) decreased with increasing furnace temperature. For [PS] = 0.02 g/cm^3, S_{BET} decreased by 8% when T increased from 114 to 133°C. For [PS] = 0.025 g/cm^3, S_{BET} decreased by 23% between the same temperatures.

Visual observations (Figs. 5–7) indicate that particle agglomeration increased with T. The higher furnace temperature heated the particles more, thus promoting faster diffusion of PS molecules and leading to significant particle adhesion and partial coalescence on the filter membrane. Partial coalescence reduced the surface area available for N_2 adsorption, resulting in lower BET surface areas despite the decrease in average particle diameter.

The variation of the ratio of S_{SEM} to S_{BET} with T (Table I) supports this picture. For particles produced at T = 114°C, S_{SEM}/S_{BET} was close to 1, suggesting that most of the SEM surface area is available for N_2 adsorption. For particles produced at T = 133°C, the ratio was significantly greater than 1, implying that N_2 could not access much of the area estimated from the particle size.

Effect of PS Concentration

The relationship between the final particle diameter and the initial PS solution concentration depends on the extent of droplet coalescence during the drying process. In the absence of droplet coalescence, we could predict the final particle size distribution from knowledge of the initial drop size distribution. A polystyrene mass balance for each spherical droplet gives

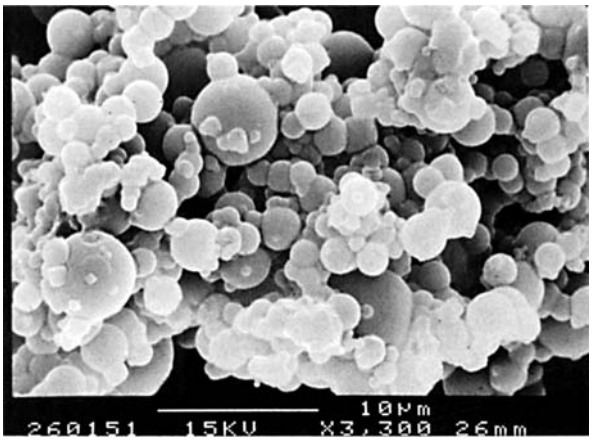

Figure 7 SEM image of PS particles produced from a solution of 280,000 g/mol PS in benzene ([PS] = 0.02 g/cm^3, Q = 124 cm^3/s, T = 147°C, and 3,300× magnification).

$$D_{PS} = D_{drop}\left(\frac{[PS]}{\rho_{PS}}\right)^{1/3} \quad (2)$$

where D_{drop} and D_{PS} are the average diameters of initial droplets and product particles, and ρ_{PS} is bulk density of PS. A log–log plot of D_{PS} vs. [PS] should have a slope of 1/3 if no droplet coalescence occurs and if D_{drop} does not depend on [PS].

Figure 8 shows the variation of average particle diameter with [PS]. The average diameters clearly increased with the polymer concentration. Barring droplet coalescence, droplets initially containing more PS produced larger solid particles. However, the slopes of the lines in Figure 8 are greater than 1/3 and imply significant droplet coalescence or dependence of D_{drop} on [PS]. The power law exponent may increase with temperature, suggesting a corresponding increase in the droplet coalescence rate, but scatter in the 133°C data preclude any firm conclusions.

Values of S_{SEM} (Table I) decreased with increasing [PS], consistent with the increase in particle diameter. The values of S_{BET} (Table I) were less than the corresponding values of S_{SEM}, perhaps due to particle aggregation and partial coalescence on the filter, which reduced the surface area available for nitrogen adsorption. On the other hand, because larger particles could have hidden some of the smaller particles, we may have systematically overestimated D_A and thus underestimated S_{SEM}.

Combining eqs. (1) and (2) and equating D_{PS} with D_A indicate that the specific surface area should be proportional to the −1/3 power of [PS] in the absence of droplet coalescence. Figure 9 shows S_{BET} as a function of [PS] and T. The slope of log(S_{BET}) vs. log([PS]) is −0.246 for T = 114°C, less in magnitude than what we would expect in the absence of coalescence. The corresponding SEM micrograph (Fig. 5) indicates little sintering of particles on the filter; hence, points of particle contact would have high radii of curvature, leading to capillary condensation of N_2 and a more gradual decrease in S_{BET} as [PS] increases and D_A decreases. For T = 133°C, the slope is −1.400, a value much greater in magnitude than −1/3. This result probably reflects particle sintering on the filter, which eliminates high curvature regions for capillary condensation and reduces the area for N_2 adsorption.

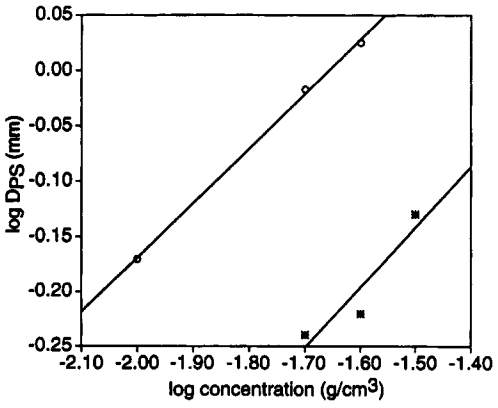

Figure 8 Dependence of area-average particle diameter (D_A) on PS concentration ([PS]) in benzene solution (Q = 124 cm³/s). Circles, T = 114°C (slope = 0.492); stars, T = 133°C (slope = 0.550).

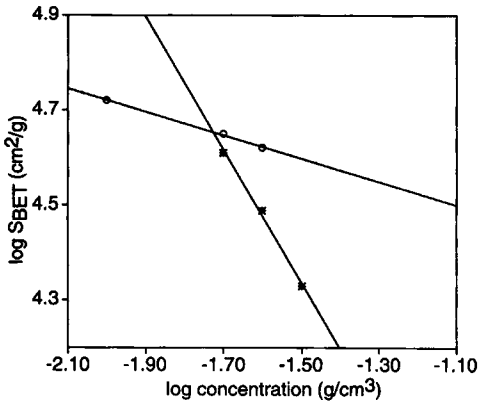

Figure 9 Dependence of BET specific surface area (S_{BET}) on PS concentration ([PS]) in benzene solution (Q = 124 cm³/s). Circles, T = 114°C (slope = −0.246); stars, T = 133°C (slope = −1.400).

The ratio S_{SEM}/S_{BET} (Table I) was about 1.5 for T = 114°C but increased significantly for T = 133°C. This difference reflects the influence of T on particle heating in the furnace followed by sintering on the filter: values of S_{SEM}/S_{BET} close to 1 imply that less sintering occurred at lower T. The value of S_{SEM}/S_{BET} should be insensitive to [PS] if particle sintering on the filter was mainly responsible for the decrease of S_{BET} relative to S_{SEM}. This seems to be the case for the lower furnace temperature.

Effect of Carrier Gas Flow Rate

Table II shows data for PS particles produced from 0.02 g/cm³ solutions of PS in benzene using different carrier gas flow rates (Q) and corresponding residence times (t) computed from Q and the volume of the furnace. The value of D_A decreased with increasing carrier gas flow rate, but the variation of D_N with Q was statistically uncertain. Thus, we shall not draw any conclusions as to the effect of Q upon the particle diameter.

Table II Effect of Carrier Gas Flow Rate on Particle Characteristics[a]

Q (cm^3/s)	τ (s)	N	D_N (μm)	D_A (μm)	S_{SEM} $(cm^2/g)/10^4$	S_{BET} $(cm^2/g)/10^4$	$\frac{S_{SEM}}{S_{BET}}$
13	35.50	949	0.71 ± 0.92	1.16 ± 1.03	4.93 ± 4.37	3.50 ± 0.07	1.41
57	8.10	811	0.73 ± 0.88	1.08 ± 0.95	5.29 ± 4.65	4.00 ± 0.02	1.32
124	3.72	548	0.66 ± 0.70	0.96 ± 0.76	5.95 ± 4.71	4.44 ± 0.02	1.34

[a] Produced from 0.02 g/cm^3 solution of PS in benzene with 114°C furnace temperature.

Values of S_{BET} significantly increased with increasing Q (Table II). After the droplets solidified into particles, their temperature certainly increased before leaving the furnace. Greater residence time in the furnace allowed the particles to gain more energy, and more of each particle probably reached a temperature greater than the PS glass transition temperature (T_g). After leaving the furnace, the hotter particles took longer to cool, thus allowing more time for partial sintering on the filter membrane. This sintering reduced the surface area available for nitrogen absorption.

The values of S_{SEM} increased with increasing Q and were higher those of S_{BET} (Table II). However, the ratio of S_{SEM} to S_{BET} did not vary with Q. The lack of clear dependence of D_A upon Q, as well as the nearly constant ratio of S_{SEM}/S_{BET} for varying Q, support the view that particle sintering on the filter membrane explains the dependence of specific surface area on Q.

Effect of Solvent Composition

Table III shows the densities, viscosities, and surface tensions of 0.02 g/cm^3 solutions of PS in various solvents, as well as the vapor pressures of the pure solvents. The solution viscosity and surface tension may influence the breakup of the liquid in the orifice of the atomizer. Lower viscosity and surface tension might produce smaller droplets and particles and may also affect the efficiency of droplet coalescence.

Table IV shows the characteristics of PS particles produced from different solvents. Particles produced from benzene and benzene-25% isopropanol had the same number-average diameter, but those produced from benzene-10% methanol and toluene were significantly smaller. Comparing the results in Table IV with the solution properties in Table III does not reveal any obvious trends. The PS particle diameter generally increased with solution viscosity, but we see no clear correlation between diameter and solution density, surface tension, or solvent vapor pressure.

SEM images (not shown) indicate that solvent composition did not have a significant effect on the particle morphology. The particles produced from all of the solvents were spherical for T = 114°C. Table IV shows that S_{BET} increased in accord with S_{SEM}. The ratio of S_{SEM} to S_{BET} was essentially independent of solvent composition, suggesting that none of the solvents plasticized the particles any more than was seen with benzene.

DISCUSSION

Characteristic Time Scales

The conversion of solution droplets into PS particles may be divided into two stages: drying in the tubular furnace, and collection on the filter membrane. Within each stage, various processes determined the

Table III Physical Properties of PS Solutions[a]

Solvent	Viscosity (cP)	Density (g/cm^3)	Surface Tension (dynes/cm)	Vapor Pressure at 114°C (atm)[b]
Benzene (BZ)	1.13 ± 0.009	0.87639 ± 0.0002	29.93 ± 0.13	2.55
BZ-25% isopropanol	1.11 ± 0.007	0.85114 ± 0.0006	26.87 ± 0.12	3.77
BZ-10% methanol	1.09 ± 0.006	0.86970 ± 0.0016	28.87 ± 0.06	5.70
Toluene	1.02 ± 0.006	0.86447 ± 0.0003	29.13 ± 0.23	1.10

[a] For 0.02 g/cm^3 solutions at 25°C.
[b] Estimated for pure solvents using the Gamma-Phi method with Antoine's Equation via THERMOPAK.

Table IV Effect of Solvent Composition on Particle Characteristics[a]

Solvent	N	D_N (μm)	D_A (μm)	S_{SEM} $(cm^2/g)/10^4$	S_{BET} $(cm^2/g)/10^4$	$\frac{S_{SEM}}{S_{BET}}$
Benzene (BZ)	949	0.71 ± 0.92	1.16 ± 1.03	4.93 ± 4.37	3.50 ± 0.07	1.41
BZ-25% isopropanol	397	0.72 ± 0.83	1.10 ± 0.91	5.19 ± 4.30	3.66 ± 0.13	1.42
BZ-10% methanol	1246	0.39 ± 0.39	0.55 ± 0.42	10.40 ± 7.93	6.57 ± 0.05	1.58
Toluene	569	0.33 ± 0.31	0.45 ± 0.33	12.70 ± 9.31	8.22 ± 0.01	1.55

[a] All produced from 0.02 g/cm^3 PS in solution, Q = 13 cm^3/s, T = 114°C.

size and morphology of the product particles. Comparing the characteristic time scales of these processes may help us gauge their relative importance in controlling the particle formation process and the final morphology of the particles.

Three processes acted in the drying stage. First, convection carried droplets through the furnace; the residence time, equal to the furnace volume divided by Q, characterized this process. Second, turbulent mixing and Brownian motion caused droplet collisions that led to coalescence as long as the droplets were liquid. Third, solvent evaporation occurred over a characteristic time that decreased as temperature increased. Our aerosolization process always produced essentially spherical PS particles with diameters that varied little with Q. These observations imply that solvent evaporation was always faster than particle convection through the furnace. The time scale of droplet collisions relative to evaporation, to be discussed shortly, influenced the average particle diameter and its distribution.

Several factors may have affected the evolution of particle morphology during the collection stage. First, prior to collection, the furnace heated the solidifying particles. The hot particles then collected on the filter membrane for up to 30 min before retrieval. During this time, significant molecular diffusion of PS could have occurred at locations where the temperature exceeded the PS glass transition temperature (T_g). PS diffusion between particles caused partial coalescence or sintering. Also, residual solvent would have plasticized the particles, lowered the T_g, and facilitated sintering. Eventually, any remaining solvent evaporated, because we did not detect residual solvent in the product particles.

Droplet Collisions vs. Evaporation

Upon entering the furnace, solvent immediately began to evaporate from the droplets. At the same time, droplets collided and coalesced with each other. An increase in the solvent evaporation rate with furnace temperature explains the corresponding decrease in the average particle diameter (Table I). Droplet collisions led to coalescence because the process reduced the total droplet surface area and decreased the aerosol's free energy. However, the probability that a collision led to coalescence decreased as the droplets solidified into particles. Because higher temperatures increased the evaporation rate, the droplets experienced fewer collisions before they solidified, thus decreasing the probability of coalescence and ultimately producing smaller solid particles.

The PS mass balance for a single droplet/particle [eq. (2)] shows that the particle diameter should scale as the 1/3 power of the initial PS solution concentration. The corresponding experimental data (Fig. 8) show that the diameter increased with [PS] more rapidly than indicated by eq. (2). This suggests that either the droplet collision rate was significant and comparable to the evaporation rate, or the aerosol's initial drop size distribution varied with [PS].

Unfortunately, we were not able to measure the drop size distribution in the aerosol produced by the atomizer. Thus, we can only speculate about the initial drop size distribution. The surface tensions and viscosities of the PS solutions varied little from those of the pure solvents, and the initial PS concentrations were probably not large enough to produce significant viscoelasticity. These observations motivate our assumption that, for a given solvent, [PS] had little effect on the initial drop size distribution produced by the atomizer.

Both Brownian motion and turbulent mixing could have caused droplet collisions. Dimensional analysis of Brownian aggregation[15] shows that the time scale t_b for two droplets to collide is given by

$$t_b = \frac{\pi \mu D^3}{8 \phi k T} \tag{3}$$

where μ, ϕ, and k are the gas viscosity, droplet volume fraction, and Boltzmann constant. For 0.5 μm

diameter droplets in an aerosol at 114°C with $\phi = 10^{-5}$, the collision time scale is on the order of 20 s, longer than the typical droplet residence time in the furnace. This suggests that droplets experienced few collisions due to Brownian motion. This leaves turbulent mixing, probably in the elbow and tube between the atomizer and the furnace, as the most likely mechanism for droplet collisions and coalescence.

Particle Solidification

The phase diagrams of polystyrene in benzene[16] and toluene[17] show that these solutions have lower critical solution temperatures (LCST) that are more than 100°C greater than the highest furnace temperatures in this study. In addition, neither solution has an upper critical solution temperature (UCST). Because our drying temperatures were always lower than the LCST, solvent evaporation did not cause phase separation. Hence, the polymer concentration profile within the droplets was always continuous, making the formation of hollow particles unlikely. The PS particles solidified by densification through the single phase region of the phase diagram.

During the densification process, the PS concentration probably remained a continuous function of position within the droplets. Like the high temperature results of Chiang and Prud'homme,[13] the smooth spherical shape and the solid internal morphology of our particles suggest that polymer inhomogeneities were small and that solvent evaporation was not diffusion limited.

The addition of a nonsolvent for PS, such as methanol or isopropanol, might have altered the phase diagram such that phase separation would occur during the drying process. Early precipitation of PS from solution, before droplet coalescence can build larger drops, might give smaller particles. The smaller particles produced from the benzene solution containing 10% methanol support this hypothesis, but the results for benzene-25% isopropanol do not. Furthermore, we cannot use the precipitation hypothesis to rationalize the small average diameter of particles produced from toluene, which has about the same solvency for PS as benzene. Further study will be needed to identify any relationship between polymer solvency and product particle size or morphology.

Particle Sintering during Collection

The extent of particle sintering on the collection filter depended on the degree to which the particles were heated above T_g while still in the furnace. Table II shows that the BET-based specific surface area decreased significantly with decreasing Q or increasing residence time. SEM images (Figs. 5–7) suggested that higher furnace temperatures led to greater neck formation and more coalescence. Longer residence times and higher furnace temperatures produced higher average particle temperatures with more of each particle at a temperature in excess of T_g. Higher particle temperatures would increase the rate and duration of PS diffusion between particles on the collection filter and, thus, decrease the surface area for N_2 adsorption. Furthermore, the duration of the experimental runs increased with decreasing carrier gas flow rate, allowing even more time for partial particle sintering due to polymer diffusion.

However, we did not observe particle melting, significant loss of spherical shape, or complete coalescence. We conclude that carrier gas was not hot enough to melt the particles, and that the residence time in the furnace was too short to allow the temperature in the particle interior to exceed T_g.

CONCLUSIONS

We used an atomizer and tubular furnace to produce colloidal PS particles from PS solutions in a variety of solvents. The average particle diameter depended on furnace temperature primarily through the solvent evaporation rate: faster evaporation solidified the droplets before many collision–coalescence events could build up the droplets' PS content. The physical properties of the initial solutions motivated our assumption that the initial drop size distribution produced by the atomizer did not vary with [PS] for a given solvent.

The carrier gas flow rate controlled the amount of heating that the particles experienced prior to collection on the filter membrane. Long residence times and high furnace temperatures led to partial heating of the particles above the T_g of PS. This enabled significant polymer diffusion between particles on the filter membrane, manifested as necking, shape distortion, and partial coalescence. Sintering could be prevented though the use of a cooling section between the furnace and the filter with admission of cool N_2 to reduce the particle temperature prior to collection.

Aerosolization and spray drying may not be the best method for producing colloidal PS particles, but the process enabled us to study the relationship between aerosolization conditions and the charac-

teristics of the product particles. This knowledge will help improve the control of spray drying processes for producing other kinds of colloidal particles that cannot be made by other methods.

REFERENCES

1. F. F. Lange, B. J. Davis, and D. O. Raleigh, *J. Am. Ceramic Soc.*, **66,** C-50 (1983).
2. I. A. Aksay, F. F. Lange, and B. I. Davis, *J. Am. Ceramic Soc.*, **66,** C-190 (1983).
3. M. D. Sacks and T. Tseng, *J. Am. Ceramic Soc.*, **67,** 526 (1984).
4. B. Fegley, P. White, and H. K. Bowen, *Ceramic Bull.*, **64,** 1115 (1985).
5. P. E. Debely, E. A. Barringer, and H. K. Bowen, *J. Am. Ceramic Soc.*, **68,** C-76 (1985).
6. W. C. Hinds, *Aerosol Technology,* Wiley, New York, 1982.
7. A. H. Lefebrve, *Atomization and Sprays,* Hemisphere, New York, 1989.
8. R. Partch, E. Matijevic, A. W. Hodgson, and B. E. Aiken, *J. Polym. Sci., Polym. Chem. Ed.*, **21,** 961 (1983).
9. K. Nakamura, R. E. Partch, and E. Matijevic, *J. Colloid Interface Sci.*, **99,** 118 (1984).
10. R. E. Partch, K. Nakamura, K. J. Wolfe, and E. Matijevic, *J. Colloid Interface Sci.*, **105,** 560 (1985).
11. D. P. Bhanti, S. K. Dua, P. Kotrappa, and N. S. Pimpale, *J. Aerosol Sci.*, **9,** 261 (1978).
12. E. Mathiowitz, H. Bernstein, S. Giannos, P. Dor, T. Turek, and R. Langer, *J. Appl. Poly. Sci.*, **45,** 125 (1992).
13. J. Chiang and R. K. Prud'homme, *J. Colloid Interface Sci.*, **122,** 283 (1988).
14. J. R. Anderson and K. C. Pratt, *Introduction to Characterization and Testing of Catalysts,* Academic Press, North Ryde, N.S.W., Australia, 1985.
15. W. B. Russel, D. A. Saville, and W. R. Schowalter, *Colloidal Dispersions,* Cambridge University, Cambridge, UK, 1989.
16. S. Saeki, N. Kuwahara, S. Konno, and M. Kaneko, *Macromolecules,* **6,** 589 (1973).
17. S. Saeki, N. Kuwahara, S. Konno, and M. Kaneko, *Macromolecules,* **6,** 246 (1973).

Received March 20, 1995
Accepted July 2, 1995